AIMS Materials Science, 12(4): 893–908.
DOI: 10.3934/matersci.2025039
Received: 11 June 2025
Revised: 31 July 2025
Accepted: 18 August 2025
Published: 05 September 2025

https://www.aimspress.com/journal/Materials

Research article

Role of hexamethylenetetramine/zinc nitrate hexahydrate molar ratio in controlling structural, morphological and optical properties of ZnO thin films synthesized by CBD

Alphonse Déssoudji Gboglo[1,2], Mazabalo Baneto[1,2,*], Ognanmi Ako[1,2], Muthiah Haris[3] and Muthusamy Senthilkuma[3]

[1] Centre d'Excellence Régional pour la Maîtrise de l'Electricité (CERME), University of Lomé, 01BP 1515, Lomé, Togo
[2] Laboratory on Solar Energy, Department of Physics, Faculty of Sciences, University of Lomé, 01BP 1515, Lomé, Togo
[3] School of Arts and Natural Sciences, Joy University, Raja Nagar, Vadakangulam, Near Kanyakumari, Tirunelveli Dist.-627116, Tamil Nadu, India

* **Correspondence:** Email: mazbaneto@gmail.com; Tel: +228-90-31-58-37.

Abstract: The present study examines the role of the hexamethylenetetramine (HMTA)-to-zinc nitrate hexahydrate (ZNH) molar ratio in controlling the physical properties of zinc oxide (ZnO) thin films obtained by chemical bath deposition (CBD) for potential applications in dye-sensitized solar cells (DSSCs). ZnO thin films were synthesized on glass substrates using aqueous solutions with different HMTA-to-ZNH molar ratios of 0, 1, 2, 3, 4, 5, and 6. The results show that this parameter strongly influences the crystallinity, morphology, and optical characteristics of the films. The X-ray diffraction analysis shows that all the ZnO thin films synthesized are polycrystalline and crystallize in a hexagonal wurtzite structure, with a fluctuating variation in crystallite size (9.5 to 43.7 nm), indicating crystal growth modulated by HMTA. The presence of characteristic functional groups and chemical bonds in ZnO thin films was confirmed by Fourier transform infrared spectroscopy. Scanning electron microscope images revealed that the molar ratio of HMTA/ZNH in the bath solution affected the morphology of the films through grain shape. The films became more compact as molar ratio increased, showing the presence of agglomerated nanotubes. UV-visible analysis showed that films obtained with HMTA/ZNH molar ratio of 4 exhibited the highest transmittance (85%) while those

elaborated without HMTA exhibited the lowest transmittance (60%) indicating the impact of HMTA on physical properties of ZnO thin films. Based on structural, morphological, and optical properties, ZnO thin films obtained with HMTA/ZNH molar ratio of 4 are more suitable to be used as a compact electron transport layer in DSSCs to limit charges recombination.

Keywords: zinc oxide; thin films; hexamethylenetetramine; zinc nitrate hexahydrate; molar ratio; chemical bath deposition

1. Introduction

Zinc oxide (ZnO) is a widely studied semiconductor material due to its excellent optoelectronic properties, including its direct band gap (3.37 eV) [1], large exciton binding energy (60 meV) [2], and high electron mobility of 205 $cm^2V^{-1}s^{-1}$ [3]. Furthermore, ZnO is an inorganic binary compound belonging to the II-VI group of semiconductors. It has a hexagonal wurtzite structure and exhibits partial polar characteristics [3]. Due to its remarkable properties, ZnO is used in various applications, including gas sensors [4], electronic devices [5,6], and photovoltaic devices, particularly dye-sensitized solar cells (DSSCs), where it serves as an alternative photoanode to titanium dioxide (TiO_2) [7]. Compared to TiO_2, ZnO offers higher electron mobility and diverse nanostructures, making it a promising alternative for improving DSSC performance [8,9]. The efficiency of DSSCs strongly depends on the structural properties of ZnO, including porosity, grain size, and texture, which influence dye adsorption and charge mobility [7]. Optimizing these parameters could improve charge transport and reduce carrier recombination. Additionally, mesoporous structures have been shown to improve the mechanical stability and adhesion of ZnO films [10]. These required properties can be achieved using the chemical bath deposition (CBD) technique and by adjusting chemicals molar ratio [11].

CBD is a simple, cost-effective, and scalable technique for synthesizing ZnO thin films with controlled morphology and crystallinity. This method is highly sensitive to several factors, including temperature, pH, deposition time, and the nature of the reagents [12]. The chemical bath composition is critical for achieving high-quality thin films, as it influences the balance between homogeneous and heterogeneous nucleation, thereby affecting ZnO growth [13]. Numerous studies have shown that the choice of precursors significantly impacts the final properties of the synthesized ZnO films [14,15]. In particular, precursor concentration and reactant molar ratios play an important role.

In the CBD technique, the hexamethylenetetramine (HMTA) is commonly used as a stabilizer. It is also reported that HMTA plays multifaceted roles in the synthesis of ZnO thin films, primarily influencing nucleation, growth kinetics, and morphological control [11,16]. However, the exact role of HMTA in ZnO growth via chemical bath deposition remains a subject of debate. Govender et al. [17] suggest that HMTA gradually releases OH^- ions through thermal decomposition, while Ashfold et al. [18] have shown that this decomposition occurs independently of ZnO synthesis reactions, confirming its role as a pH buffer. Sugunan et al. [19] challenge this hypothesis, proposing that HMTA acts primarily as a chelating agent, directing anisotropic ZnO growth. Conversely, McPeak et al. [20] argue that HMTA does not adsorb onto the lateral facets of ZnO and serves only to regulate OH^- concentration. Finally, Strano et al. [21] propose that HMTA plays a dual role, both as an OH^- supplier and as a growth-directing agent that promotes anisotropic ZnO formation.

Given the significance of these growth mechanisms, this study investigates the influence of the HMTA-to-zinc nitrate hexahydrate (ZNH) molar ratio on the physical properties of ZnO thin films. The research work focuses on how HMTA/ZNH molar ratio affects the structural, morphological, and optical properties of ZnO films, aiming to identify optimal synthesis conditions for photovoltaic applications.

2. Materials and methods

2.1. Materials and reagents

In this work, ZnO thin films were synthesized using the CBD method. The microscopic glass slides were used as a substrate for synthesizing different ZnO thin films. All the employed chemical materials, such as ZNH and HMTA, were obtained from Isochem Laboratory and sodium hydroxide pellets from Merck in India. All analytical grade (AR) chemicals were utilized without further treatment. Ethanol (99.9%), acetone, and distilled water was used during the present research work.

2.2. Synthesis of ZnO thin films

The glass substrates were cleaned in an ultrasonic bath with acetone, ethanol, and distilled water for 15 min each, followed by drying in nitrogen (N_2). The bath solution was obtained by mixing HMTA and ZNH. Different deposition solutions were prepared by varying HMTA-to-ZNH molar ratios (0, 1, 2, 3, 4, 5 and 6), with a fixed zinc concentration of 0.1 M. Each solution was prepared by dissolving the appropriate amounts of HMTA and ZNH in distilled water, yielding a final volume of 150 mL. The solutions were homogenized using a magnetic stirrer, and sodium hydroxide was gradually added to adjust the pH to 8, turning the solution milky white. Deposition was conducted at 65 °C under continuous stirring. The cleaned glass substrates were immersed vertically in the bath, ensuring they did not touch the beaker's sides. After a 20 min deposition, the substrates were removed and air-dried. Finally, the ZnO-coated films were annealed at 400 °C for 3 h. The samples obtained with HMTA/ZNH ratio of 0, 1, 2, 3, 4, 5, and 6 were designated as H0, H1, H2, H3, H4, H5, and H6, respectively.

2.3. ZnO thin films Characterization

The structural properties of the synthesized ZnO thin films were analyzed using an X-ray diffractometer (EMPYREAN model) with Cu-Kα radiation (λ = 1.54059 Å), scanning over a 2θ range of 10° to 90° at room temperature. The surface morphology was examined with a ZEISS EVO 18 scanning electron microscope (SEM) operated at 10 kV. To enhance conductivity, the samples were carbon-coated due to the insulating nature of the glass substrate. The optical properties were assessed using a UV-Vis-NIR spectrophotometer (PerkinElmer LAMBDA model), scanning between 300 and 900 nm. The presence of specific functional groups in the ZnO films was analyzed through Fourier transform infrared (FTIR) spectroscopy (Perkin-Elmer Spectrum 3 model), equipped with an attenuated total reflectance (ATR) accessory. Measurements were conducted in transmission mode over the 400–4000 cm^{-1} range, with a spectral resolution of 4 cm^{-1}. The data presented in this study represent the average of 10 scans.

3. Results and discussion

3.1. Structural characterization

The X-ray diffraction (XRD) spectra of ZnO thin films, obtained for different molar ratios of HMTA/ZNH are shown in Figure 1. All diffraction peaks detected at 2θ angles greater than 30° correspond to the hexagonal wurtzite $P6_3mc$ structure of ZnO, in accordance with JCPDS card 36-1451 [22].

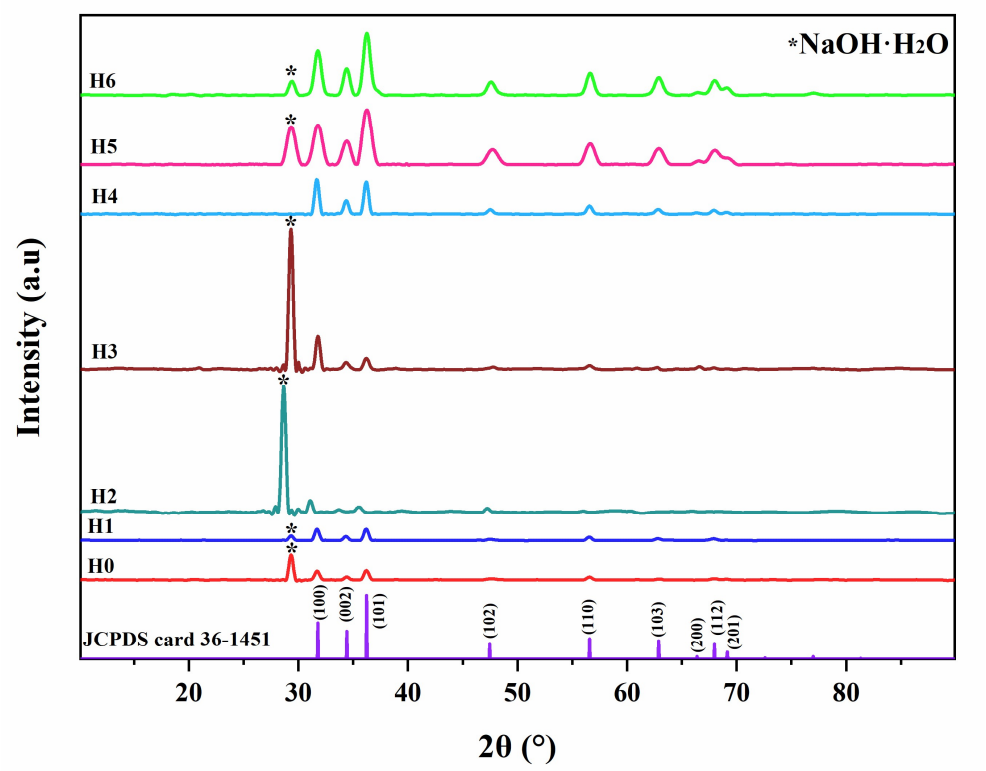

Figure 1. XRD patterns of ZnO thin films obtained for different molar ratios of HMTA/ZNH.

Figure 1 also reveals the presence of impurity diffraction peaks around 29° for most samples, indicating the formation of sodium hydroxide monohydrate ($NaOH{\cdot}H_2O$) [23]. This impurity may result from incomplete dissolution of NaOH in distilled water [24,25]. However, no impurity peaks were observed for sample H4 (molar ratio 4), suggesting higher crystalline purity for this ratio.

To assess the degree of preferential orientation of the crystallites from the peak intensities, the texture coefficient ($T_{C(hkl)}$) was calculated for the first three peaks showing the highest intensity based on Eq 1 [26]:

$$T_{C(hkl)} = \frac{\frac{I_{(hkl)}}{I_{0(hkl)}}}{\frac{1}{n}\sum \frac{I_{(hkl)}}{I_{0(hkl)}}} \quad (1)$$

where $I_{(hkl)}$ are the XRD intensities obtained from the films, n the number of diffraction peaks considered and $I_{0(hkl)}$ are the intensities of the XRD reference (JCPDS card 36-1451) of the randomly oriented grains.

As shown in Table 1, the analysis of crystallite growth rates along the (100), (002), and (101) planes reveals a progressive preferential growth along the (100) plane, reaching a maximum at molar ratio 2 (sample H2). This is followed by a decline at molar ratio 3 (sample H3), and subsequently by increasingly disordered growth for higher molar ratios (4 to 6). This behavior can be attributed to anisotropic crystallite growth, influencing the density of ZnO structures through modifications in the nucleation process favored by HMTA [27]. The sharp and well-defined diffraction peaks confirm the high crystallinity of the ZnO thin films.

The plane d-spacing (d) and the lattice parameters (a and c) of the synthesized ZnO thin films were calculated according to Bragg's law Eqs 2 and 3, respectively [28]:

$$d = \frac{\lambda}{2\sin\theta} \tag{2}$$

$$a = \sqrt{\frac{1}{3}}\frac{\lambda}{\sin\theta} \text{ and } c = \frac{\lambda}{\sin\theta} \tag{3}$$

where λ is Cu-Kα wavelength (1.54059 Å) and θ is the diffraction peak angle.

The calculated lattice parameters (a and c) and interplanar spacings (d) for the (100), (002), and (101) planes, reported in Table 1, are very close to the standard values from JCPDS card 36-1451 for ZnO. The c/a ratio remains nearly constant, around 1.60 for all samples, which is characteristic of the wurtzite structure and suggests compact films.

The crystallite size (D) of the films along the dominant peaks (100), (002) and (101) was calculated using Debye Scherer formula (Eq 4) [29]:

$$D = \frac{k\lambda}{\beta\cos\theta} \tag{4}$$

where $k = 0.9$, θ is the XRD diffraction peak angle, $\lambda = 1.5406$ Å is the X-ray wavelength and β is the full width at half peak (FWHM) in radians. The dislocation density (δ) which induces the impurities (defects) in crystal is estimated by Eq 5 [29]:

$$\delta = \frac{1}{D^2} \tag{5}$$

Table 1. Texture coefficient, lattice parameters and structural characteristics of ZnO thin films obtained for different molar ratios of HMTA/ZNH along the dominant peaks (100), (002) and (101).

Samples	hkl	2θ (°)	$T_{C(hkl)}$	FWHM (°)	D (nm)	δ ($\times 10^{15}$ lines/m^2)	d (Å)	Lattice parameters (Å)		c/a ratio
								a	c	
H0	100	31.707	1.5	0.490	16.854	3.520	2.820	3.256	5.210	1.600
	002	34.401	0.6	0.432	19.251	2.698	2.605			
	101	36.205	0.9	0.487	17.162	3.395	2.479			
H1	100	31.688	1.5	0.462	17.875	3.130	2.821	3.258	5.219	1.602
	002	34.337	0.7	0.458	18.155	3.034	2.610			
	101	36.180	0.9	0.476	17.558	3.244	2.481			
H2	100	31.091	2.3	0.301	27.395	1.332	2.874	3.319	5.317	1.602
	002	33.683	0.3	0.265	31.322	1.019	2.659			
	101	35.529	0.4	0.340	24.535	1.661	2.525			
H3	100	31.800	2.1	0.189	43.705	0.524	2.812	3.247	5.218	1.607
	002	34.347	0.5	0.294	28.282	1.250	2.609			
	101	36.192	0.5	0.374	22.347	2.002	2.480			
H4	100	31.679	1.4	0.454	18.189	3.023	2.822	3.259	5.216	1.600
	002	34.361	0.8	0.496	16.765	3.558	2.608			
	101	36.190	0.8	0.479	17.448	3.285	2.480			
H5	100	31.770	1.2	0.870	9.494	11.095	2.814	3.250	5.211	1.603
	002	34.394	0.8	0.766	10.856	8.484	2.605			
	101	36.253	1.0	0.875	9.553	10.957	2.476			
H6	100	31.771	1.2	0.701	11.783	7.203	2.814	3.250	5.210	1.603
	002	34.397	0.8	0.639	13.014	5.904	2.605			
	101	36.251	1.0	0.736	11.357	7.752	2.476			
JCPDS	100	31.770	-	-	-	-	2.814	3.250	5.207	1.602
card 36-1451	002	34.422	-	-	-	-	2.603			
	101	36.253	-	-	-	-	2.476			

The values of FWHM, crystallite size, and dislocation density for the (100), (002), and (101) planes were reported in Table 1 for different HMTA/ZNH molar ratios. The variation in FWHM across the three crystallographic planes exhibits a non-linear trend, alternating between decreasing and increasing values To better visualize their variations, the crystallite size and dislocation density were plotted as a function of molar ratio and presented in Figure 2. As shown in Figure 2a, the crystallite size increases with the molar ratio up to a value of 3, then decreases beyond this point. This fluctuation may be attributed to the progressive agglomeration of ZnO nanostructures at higher HMTA concentrations, which promotes non-uniform nucleation and growth, leading to broader crystallite size distributions and increased microstrain. Simultaneously, dislocation density follows an inverse trend, increasing as crystallite size decreases (Figure 2b). These results emphasize the critical role of the

HMTA/ZNH molar ratio in controlling the structural quality of ZnO nanostructures synthesized via chemical bath deposition.

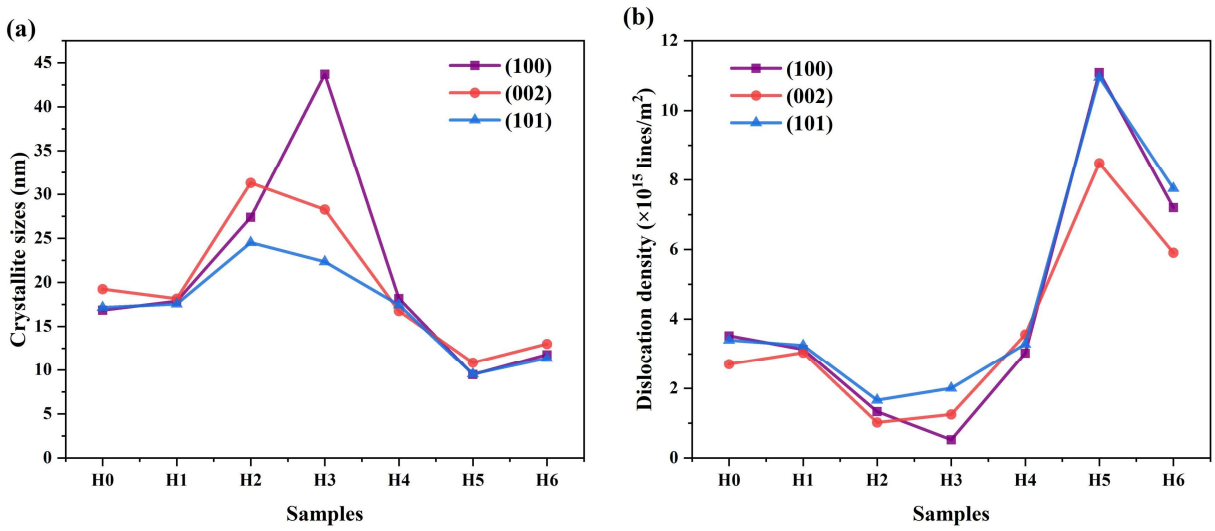

Figure 2. (a) Crystallites size and (b) dislocation density for different molar ratios of HMTA/ZNH along the dominant peaks (100), (002) and (101).

3.2. Morphological properties

Figure 3 presents SEM images for different molar ratios of HMTA/ZNH. These results show that HMTA concentration in the deposition solution significantly influences the thin film morphology, affecting grain shape, size, and distribution. As the molar ratio increases, the films become more compact, exhibiting a morphological transition from loosely arranged elliptical aggregates to densely packed and agglomerated nanospheres. The grain size increases up to a molar ratio of 3 (sample H3), before decreasing at higher ratios, suggesting the presence of a threshold effect linked to HMTA concentration. This behavior can be attributed to the dual role of HMTA as a slow OH^- ion releaser and a structure-directing agent during the chemical bath deposition process [21]. Up to a certain concentration, HMTA facilitates controlled nucleation and crystal growth. However, beyond a molar ratio of 3, excessive HMTA likely leads to oversaturation of complexing agents, reducing the availability of free Zn^{2+} and OH^- ions, and thus hindering further crystal growth. The ZnO thin films obtained without HMTA exhibited small grains, similar to those observed at higher HMTA/ZNH ratios (above 3), further supporting the hypothesis of limited crystal development under HMTA-deficient or HMTA-saturated conditions. These morphological observations are in good agreement with XRD results and highlight the strong influence of the HMTA/ZNH molar ratio on ZnO crystal growth and structural evolution.

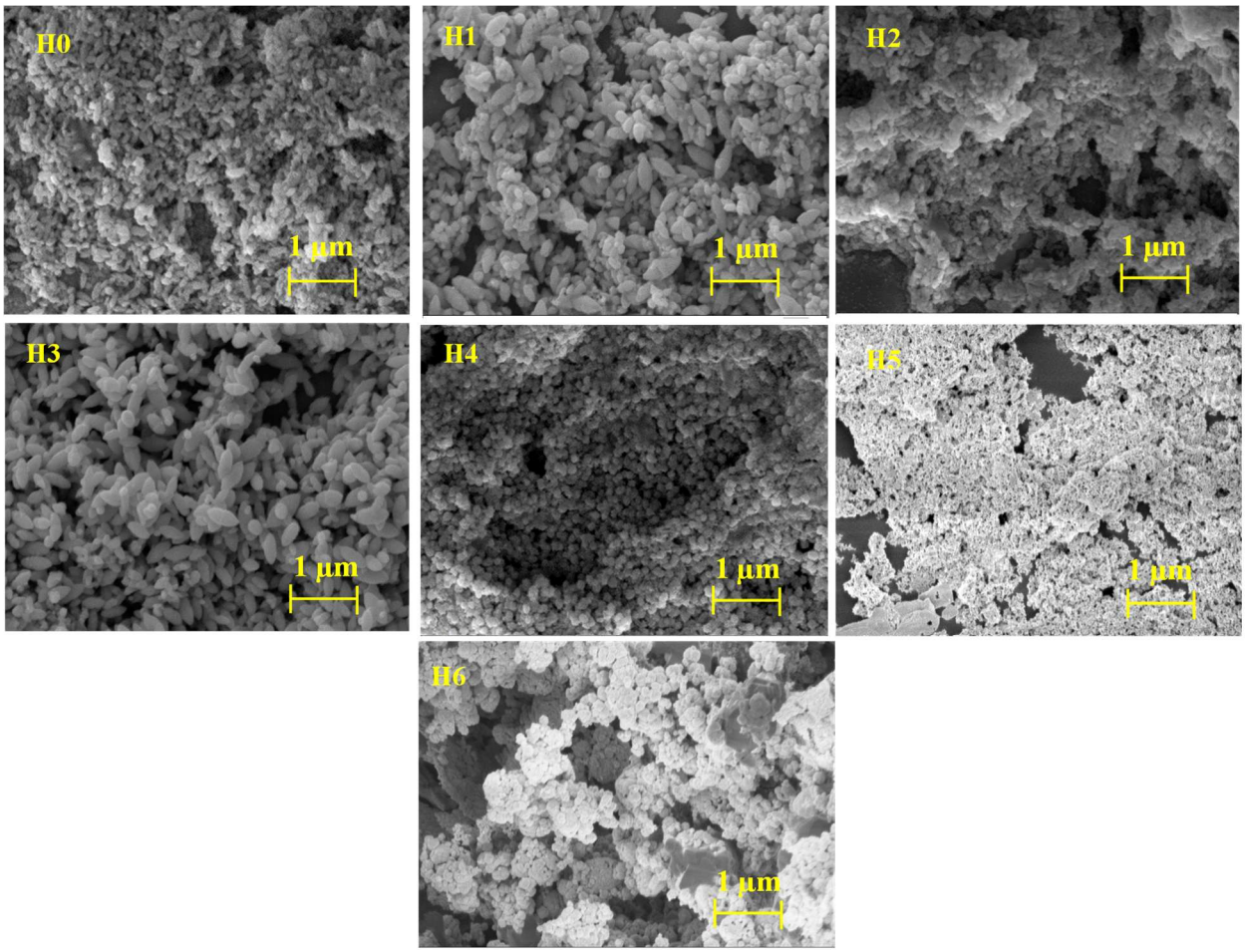

Figure 3. SEM images of ZnO thin films obtained for different molar ratios of HMTA/ZNH.

Based on morphological observations, samples H1 (molar ratio 1) and H3 (molar ratio 3) appear to be a promising candidate for DSSC applications. Their dense and uniform films composed of elliptically shaped nanoparticles suggests a favorable structure for efficient electron transport [7]. Their porous structures and high specific surface area are expected to enhance dye adsorption and electron transport which are the key factors in improving the energy conversion efficiency of DSSCs [30]. Moreover, sample H4 displays a compact surface morphology composed of well-defined nanospheres. This type of structure may reduce dye adsorption capacity due to a lower specific surface area but could be advantageous as a compact electron transport layer in DSSC configurations requiring limited recombination [7,30]. These observations suggest that tuning the HMTA/ZNH molar ratio has a direct impact on the final ZnO film morphology, allowing the material to be tailored for specific roles within DSSC devices.

3.3. FTIR analysis

Figure 4 presents the FTIR spectra of ZnO thin films synthesized at different HMTA/ZNH molar ratios, highlighting several characteristic absorption bands. The Zn–O vibrational modes observed around 420 cm^{-1} confirm the formation of ZnO for all samples, consistent with our previous works [31,32].

The variation in intensity of these bands suggests differences in particle growth dynamics, which is consistent with the morphological and structural trends revealed by SEM and XRD analyses.

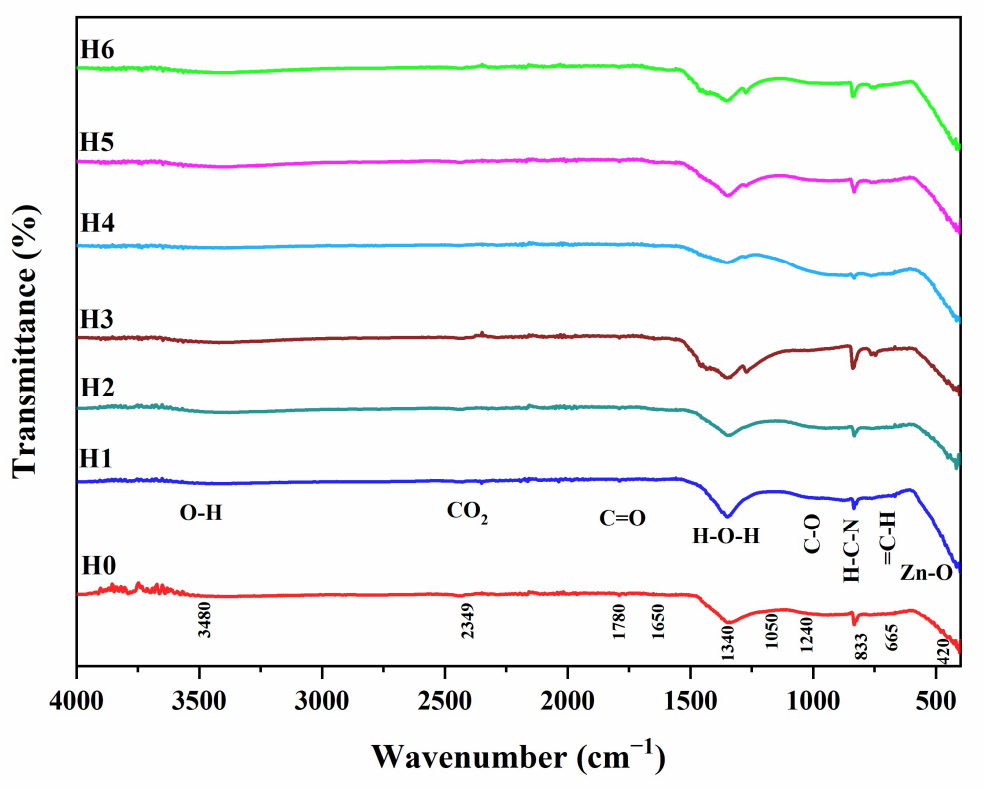

Figure 4. FTIR spectrum of ZnO thin films obtained for different molar ratios of HMTA/ZNH.

A band near 665 cm^{-1} corresponds to =C–H bending, while a peak around 833 cm^{-1} is attributed to H–C–N stretching, likely originating from residual HMTA or its interaction products with the solution [33]. C–O stretching vibrations of primary alcohols are detected between 1240 and 1050 cm^{-1} [34]. A pronounced absorption around 1380 cm^{-1}, assigned to H–O–H bending, reflects traces of adsorbed water within the ZnO matrix [35], while bands between 1780 and 1650 cm^{-1} correspond to C=O stretching vibrations of amide groups I and II. The peak at 2349 cm^{-1} is associated with atmospheric CO_2 molecules [36], and the broad band centered around 3480 cm^{-1} corresponds to O–H stretching vibrations, due to hydroxyl groups or physisorbed water [37].

Interestingly, these organic- and moisture-related bands (=C–H, H–C–N, H–O–H) are noticeably weaker in the spectrum of sample H4, suggesting a lower content of residual organics. This observation is consistent with the XRD analysis, which shows no impurity phases for H4. In contrast, other samples, particularly those synthesized with higher HMTA concentrations, exhibit stronger bands in these regions, indicating greater incorporation of organic residues during growth. These results confirm that the chemical composition and surface purity of the ZnO films are influenced by the HMTA/ZNH molar ratio, which affects both structural and surface characteristics of the thin films.

3.4. Optical properties

Figure 5 presents the optical transmittance of ZnO thin films obtained with different molar ratios of HMTA/ZNH. It is observed that films synthesized with a molar ratio of 4 exhibit the highest transmittance, reaching 85% in the visible region, while those prepared without HMTA show a lower transmittance of around 60%.

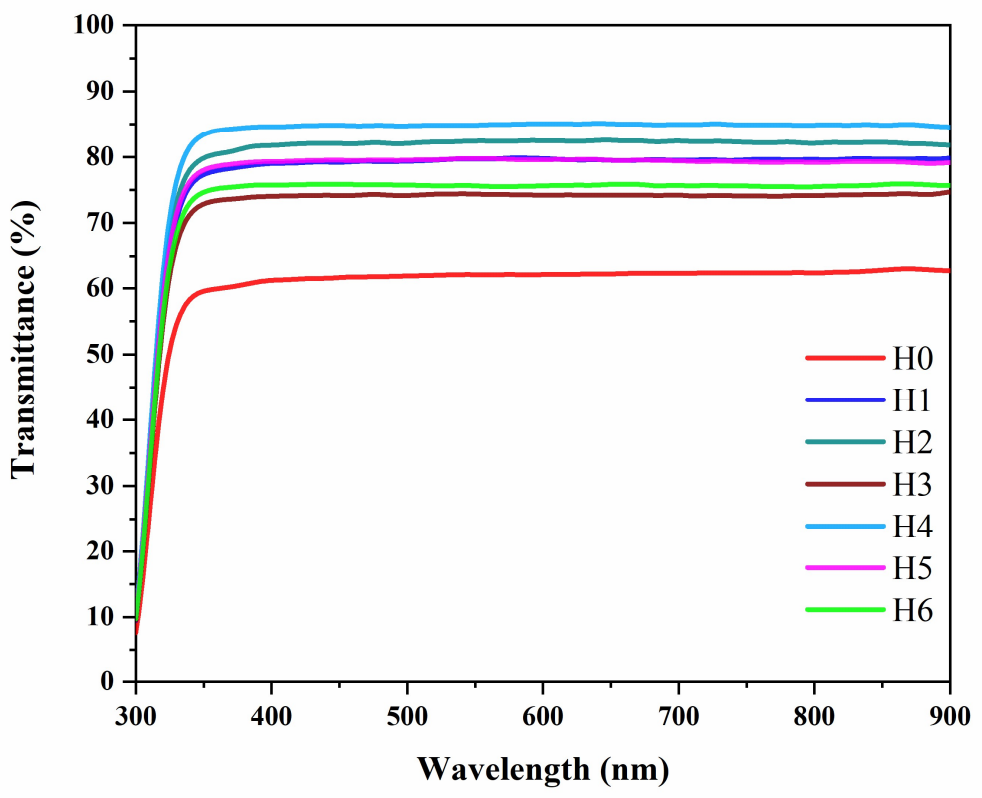

Figure 5. Optical transmittance spectrum of ZnO thin films obtained for different molar ratios of HMTA/ZNH.

This improvement in transmittance for the molar ratio of 4 can be correlated with the XRD and SEM results. XRD analysis revealed that sample H4 (molar ratio of 4) has a well-defined crystalline structure with no impurity peaks, indicating higher crystal purity and fewer defects, which enhances light transmission. Additionally, SEM images shown that ZnO films synthesized with a molar ratio of 4 exhibit homogeneous and compact morphology, with well-formed small grains. These structural and morphological properties explain the reduced unwanted light scattering and absorption, contributing to the high transmittance of these films. The lowed transmittance observed for samples H1 and H3 (80% and 74%, respectively) maybe due to the light scattering as SEM images showed agglomerated large grains.

The band-gap energy of the deposited ZnO films was determined (Figure 6) using Tauc's relation as shown by Eq 6 [38]:

$$(\alpha h\upsilon)^n = A(h\upsilon - E_g) \tag{6}$$

where α, n, E_g, and $h\upsilon$ are the absorption coefficient, power factor of the transition mode, band-gap energy, and photon energy, respectively.

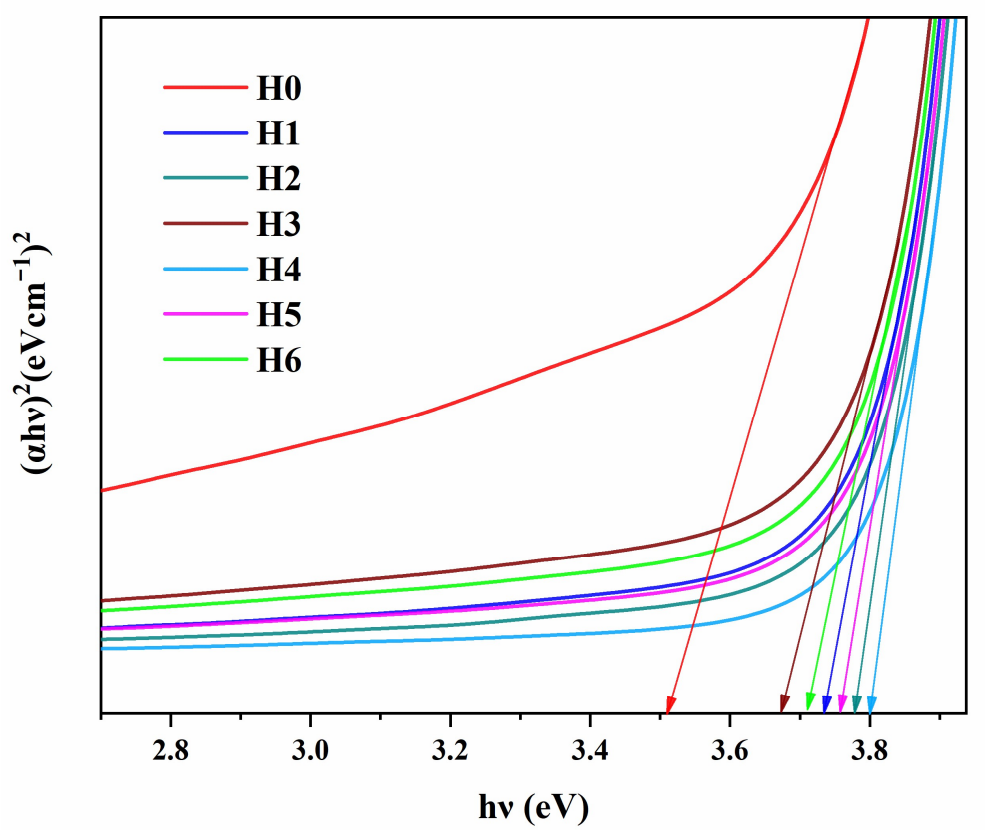

Figure 6. Optical band gap variations in ZnO thin films obtained for different molar ratios of HMTA/ZNH.

The optical energy band gaps (E_g) for different HMTA/ZNH molar ratios were estimated by extrapolating the linear region of the Tauc plot, as shown in Figure 6. The E_g values for ZnO thin films range between 3.51 and 3.80 eV. These values are higher than the typical band gap of bulk ZnO, which is around 3.37 eV [1]. Such an increase is commonly attributed to internal stresses in the film, quantum confinement effects due to small grain size, and structural disorder [39,40]. SEM and XRD results show that smaller grains, typically obtained at higher HMTA concentrations, enhance the quantum confinement effect and lead to higher E_g values. In contrast, larger grains reduce this effect, resulting in lower E_g values [41]. The possible presence of impurity phases from NaOH ($NaOH{\cdot}H_2O$) or residual chemical species from HMTA may also alter the band structure and contribute to the observed variations in the band-gap energy. A disorder, known as Urbach's tail, which is related to the width of localized states available in the optical bandgap of ZnO thin films [42], has been studied for further investigation. The Urbach energy (E_u) was determined from the slope of the straight line obtained by plotting ln(α) as a function of incident photon energy hυ (Figure 7) [42]. The results reveal that E_g fluctuations are directly correlated with those of E_u (Figure 8), indicating that defects and crystal disorder significantly influence bandgap modifications [43]. These results are consistent with previous reports in the literature on ZnO thin films grown under different conditions [31,34,43,44].

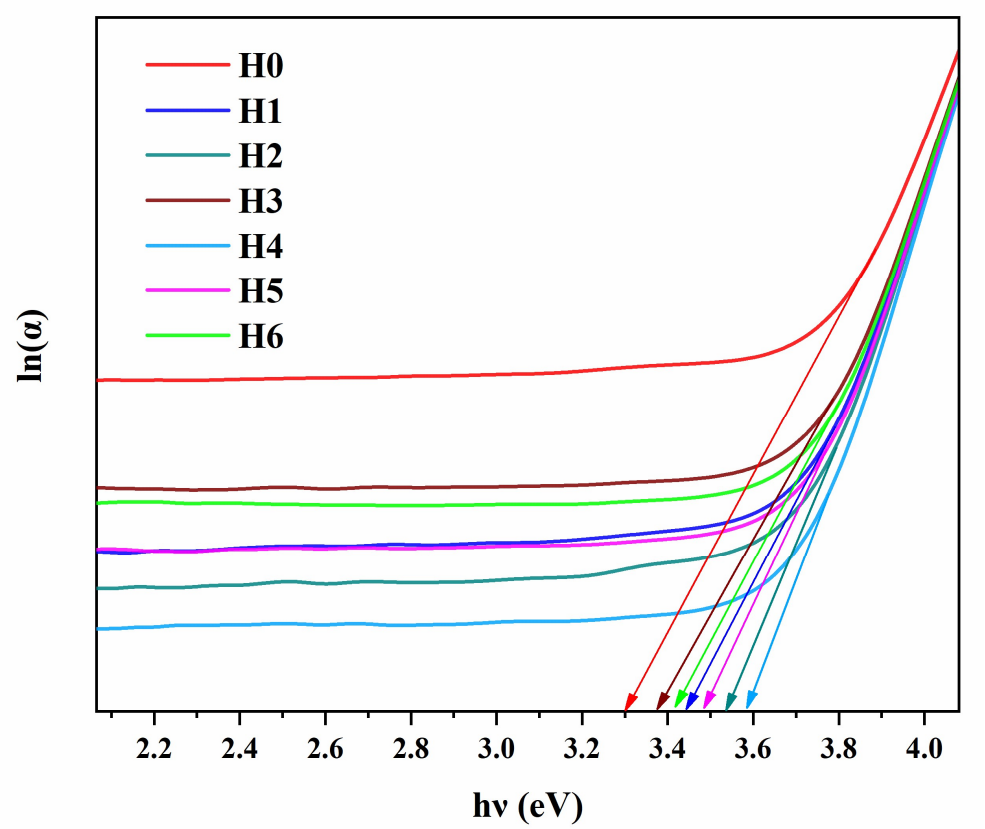

Figure 7. Plot of ln(α) versus hυ for the determination of the Urbach energy of ZnO thin films obtained for different molar ratios of HMTA/ZNH.

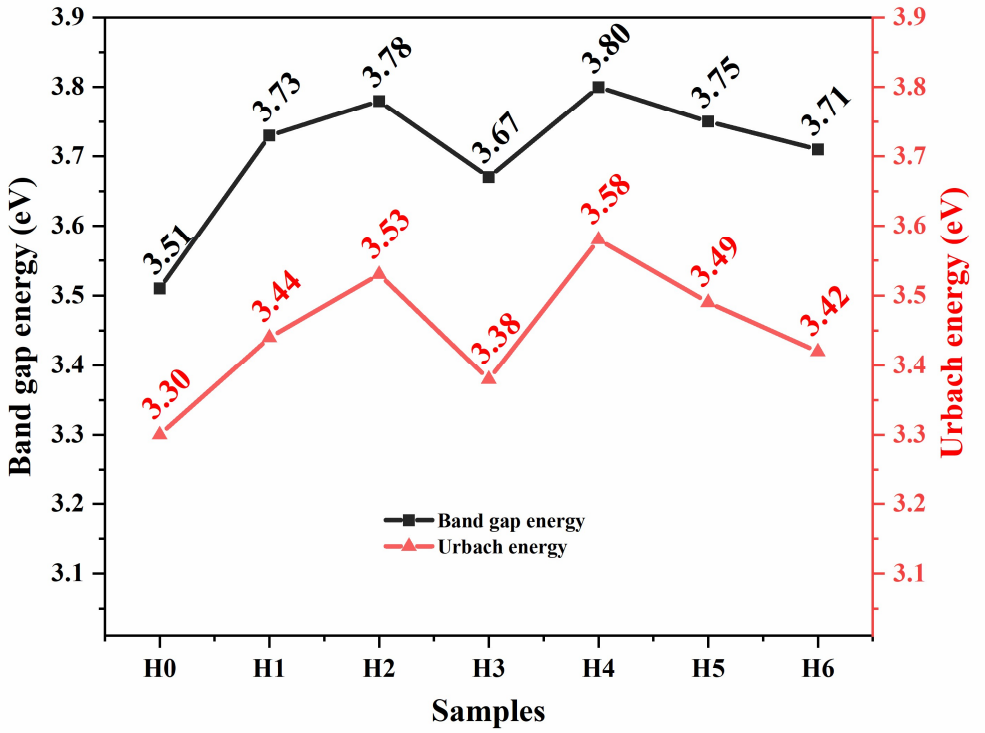

Figure 8. Band gap energy and Urbach energy values for ZnO thin films obtained for different molar ratios of HMTA/ZNH.

4. Conclusions

This study highlights the influence of the HMTA-to-ZNH molar ratio on the physical properties of ZnO thin films synthesized by CBD. The results show that molar ratio variations significantly impact the crystallinity, morphology and optical characteristics of the films. X-ray diffraction analysis reveals that crystallite size varies non-linearly as a function of HMTA/ZNH molar ratio, suggesting agglomerate growth favored by HMTA. Scanning electron microscopy imaging shows that HMTA concentration directly influences film morphology. An increase in the molar ratio leads to more compact structures and favors the formation of agglomerated nanotubes. Fourier transform infrared spectroscopy confirms the presence of functional groups and chemical bonds characteristic of ZnO. Optical measurements indicate that the band gap of ZnO thin films varies between 3.51 and 3.80 eV. The films obtained with a molar ratio of 4 show the highest transmittance (85%), while those synthesized without HMTA display the lowest (60%) transmittance in the visible region, indicating the impact of HMTA on the optical properties of ZnO thin films. Among the synthesized samples, the one obtained with molar ratio of 4 (HMTA/ZNH = 4) exhibited the optimal structural, morphological, and optical properties, being consequently more suitable for DSSC applications.

Use of AI tools declaration

The authors declare they have not used Artificial Intelligence (AI) tools in the creation of this article.

Acknowledgments

This research is supported by the Centre d'Excellence Régional pour la Maîtrise de l'Électricité (CERME) and FICCI DST (India) through the CV Raman International Fellowship Program for African Researchers (DST/INT/CVRF/2022).

Author contributions

Conceptualization: A. D. Gboglo and M. Baneto; methodology: A. D. Gboglo and M. Baneto; formal analysis: O. Ako, M. Haris, and M. Senthilkumar; writing—original draft: A.D. Gboglo; supervision: M. Baneto; writing—review and editing: M. Baneto, O. Ako, M. Haris, and M. Senthilkumar. All authors have read and agreed to the published version of the manuscript.

Conflict of interest

The authors declare no conflict of interest.

References

1. Parihar V, Raja M, Paulose R (2018) A brief review of structural, electrical and electrochemical properties of zinc oxide nanoparticles. *Rev Adv Mater Sci* 53: 119–130. https://doi.org/10.1515/rams-2018-0009

2. Hassan NK, Hashim MR, Al-Douri Y (2014) Morphology and optical investigations of ZnO pyramids and nanoflakes for optoelectronic applications. *Optik* 125: 2560–2564. https://doi.org/10.1016/j.ijleo.2013.10.023
3. Look DC, Reynolds DC, Sizelove JR, et al. (1998) Electrical properties of bulk ZnO. *Solid State Commun* 105: 399–401. https://doi.org/10.1016/S0038-1098(97)10145-4
4. Zhang N, Yu K, Li L, et al. (2008) Investigation of electrical and ammonia sensing characteristics of Schottky barrier diode based on a single ultra-long ZnO nanorod. *Appl Surf Sci* 254: 5736–5740. https://doi.org/10.1016/j.apsusc.2008.03.039
5. Arnold MS, Avouris P, Pan ZW, et al. (2003) Field-effect transistors based on single semiconducting oxide nanobelts. *J Phys Chem B* 107: 659–663. https://doi.org/10.1021/jp0271054
6. Rodnyi PA, Khodyuk IV (2011) Optical and luminescence properties of zinc oxide (Review). *Opt Spectrosc* 111: 776–785. https://doi.org/10.1134/S0030400X11120216
7. Vittal R, Ho KC (2017) Zinc oxide based dye-sensitized solar cells: A review. *Renew Sust Energ Rev* 70: 920–935. https://doi.org/10.1016/j.rser.2016.11.273
8. Tyona MD, Osuji RU, Ezema FI (2013) A review of zinc oxide photoanode films for dye-sensitized solar cells based on zinc oxide nanostructures. *Adv Nano Res* 1: 43–58. https://doi.org/10.12989/ANR.2013.1.1.043
9. Liu Z, Liu C, Ya J, et al. (2011) Controlled synthesis of ZnO and TiO_2 nanotubes by chemical method and their application in dye-sensitized solar cells. *Renew Energ* 36: 1177–1181. https://doi.org/10.1016/j.renene.2010.09.019
10. Guillén E, Azaceta E, Vega-Poot A, et al. (2013) ZnO/ZnO core–shell nanowire array electrodes: Blocking of recombination and impressive enhancement of photovoltage in dye-sensitized solar cells. *J Phys Chem C* 117: 13365–13373. https://doi.org/10.1021/jp402888y
11. Lausecker C, Salem B, Baillin X, et al. (2023) Effects of zinc nitrate and HMTA on the formation mechanisms of ZnO nanowires on Au seed layers. *Cryst Growth Des* 23: 2941–2950. https://doi.org/10.1021/acs.cgd.3c00068
12. Fekadu GH, Tizazu A (2019) Short review of factors affecting chemical bath deposition method for metal chalcogenide thin films. *Int J Thin Fil Sci Tec* 8: 43–53. http://dx.doi.org/10.18576/ijtfst/080203
13. Drici A, Djeteli G, Tchangbedji G, et al. (2004) Structured ZnO thin films grown by chemical bath deposition for photovoltaic applications. *Phys Stat Sol A* 201: 1528–1536. https://doi.org/10.1002/pssa.200306806
14. Bacaksiz E, Parlak M, Tomakin M, et al. (2008) The effects of zinc nitrate, zinc acetate and zinc chloride precursors on investigation of structural and optical properties of ZnO thin films. *J Alloys Compd* 466: 447–450. https://doi.org/10.1016/j.jallcom.2007.11.061
15. Baneto M, Enesca A, Lare Y, et al. (2014) Effect of precursor concentration on structural, morphological and opto-electric properties of ZnO thin films prepared by spray pyrolysis. *Ceram Int* 40: 8397–8404. https://doi.org/10.1016/j.ceramint.2014.01.048
16. Aris SNM, Azmi ZH, Sagadevan S, et al. (2023) Effect of hexamethylenetetramine of zinc oxide nanowires using chemical bath deposition method. *Cryst Res Technol* 58: 2300075. https://doi.org/10.1002/crat.202300075

17. Govender K, Boyle DS, Kenway PB, et al. (2004) Understanding the factors that govern the deposition and morphology of thin films of ZnO from aqueous solution. *J Mater Chem* 14: 2575–2591. https://doi.org/10.1039/B404784B
18. Ashfold MNR, Doherty RP, Ndifor-Angwafor NG, et al. (2007) The kinetics of the hydrothermal growth of ZnO nanostructures. *Thin Solid Films* 515: 8679–8683. https://doi.org/10.1016/j.tsf.2007.03.122
19. Sugunan A, Warad HC, Boman M, et al. (2006) Zinc oxide nanowires in chemical bath on seeded substrates: Role of hexamine. *J Sol-Gel Sci Technol* 39: 49–56. https://doi.org/10.1007/s10971-006-6969-y
20. McPeak KM, Le TP, Britton NG, et al. (2011) Chemical bath deposition of ZnO nanowires at near-neutral pH conditions without hexamethylenetetramine (HMTA): Understanding the role of HMTA in ZnO nanowire growth. *Langmuir* 27: 3672–3677. https://doi.org/10.1021/la105147u
21. Strano V, Urso RG, Scuderi M, et al. (2014) Double role of HMTA in ZnO nanorods grown by chemical bath deposition. *J Phys Chem C* 118: 28189–28195. https://doi.org/10.1021/jp507496a
22. McMurdie HF, Morris MC, Evans EH, et al. (1986) Standard X-ray diffraction powder patterns from the JCPDS research associateship. *Powder Diffr* 1: 64–77. https://doi.org/10.1017/S0885715600011593
23. Koliverdov VF (2010) Relation between the temperature coefficient of surface tension and phase diagrams. *Russ J Phys Chem* 84: 1294–1300. https://doi.org/10.1134/S0036024410080042
24. Wunderlich JA (1958) Contribution à l'étude cristallochimique des hydrates de soude. I.—Méthodes expérimentales et les structures cristallines de $NaOH·H_2O$ et de $2NaOH·7H_2O$. *Bull Mineral* 81: 287–314. https://doi.org/10.3406/bulmi.1958.5288
25. Hemily PW (1957) Structures cristallines des hydrates de la soude. I. Structure cristalline de $NaOH·4H_2O$. *Acta Cryst* 10: 37–44. https://doi.org/10.1107/S0365110X57000092
26. Romero R, Leinen D, Dalchiele EA, et al. (2006) The effects of zinc acetate and zinc chloride precursors on the preferred crystalline orientation of ZnO and Al-doped ZnO thin films obtained by spray pyrolysis. *Thin Solid Films* 515: 1942–1949. https://doi.org/10.1016/j.tsf.2006.07.152
27. Parize R, Garnier J, Chaix-Pluchery O, et al. (2016) Effects of hexamethylenetetramine on the nucleation and radial growth of ZnO nanowires by chemical bath deposition. *J Phys Chem C* 120: 5242–5250. https://doi.org/10.1021/acs.jpcc.6b00479
28. Kashif M, Hashim U, Ali ME, et al. (2012) Effect of different seed solutions on the morphology and electrooptical properties of ZnO nanorods. *J Nanomater* 2012: 452407. https://doi.org/10.1155/2012/452407
29. Mustapha S, Ndamitso MM, Abdulkareem AS, et al. (2019) Comparative study of crystallite size using Williamson-Hall and Debye-Scherrer plots for ZnO nanoparticles. *Adv Nat Sci Nanosci Nanotechnol* 10: 045013. https://doi.org/10.1088/2043-6254/ab52f7
30. Kanmani SS, Ramachandran K (2013) Role of aqueous ammonia on the growth of ZnO nanostructures and its influence on solid-state dye sensitized solar cells. *J Mater Sci* 48: 2076–2091. https://doi.org/10.1007/s10853-012-6981-2
31. Gboglo AD, Baneto M, Gadedjisso-Tossou KS, et al. (2025) Co-effect of pH control agent and pH value on the physical properties of ZnO thin films obtained by chemical bath deposition for potential application in dye-sensitized solar cells. *Surfaces* 8: 46. https://doi.org/10.3390/surfaces8030046

32. Ako O, Baneto M, Senthilkumar M, et al. (2025) Simultaneous effect of precursor sources and precursor concentration on structural, morphological and optical properties of ZnO nanostructured thin films for photovoltaic applications. *Int J Renewable Energy Dev*. https://doi.org/10.61435/ijred.2025.61069
33. Idiawati R, Mufti N, Taufiq A, et al. (2017) Effect of growth time on the characteristics of ZnO nanorods. *IOP Conf Ser Mater Sci Eng* 202: 012050. https://doi.org/10.1088/1757-899X/202/1/012050
34. Jahan Tamanna N, Sahadat Hossain Md, Mohammed Bahadur N, et al. (2024) Green synthesis of Ag_2O & facile synthesis of ZnO and characterization using FTIR, bandgap energy & XRD (Scherrer equation, Williamson-Hall, size-train plot, Monshi- Scherrer model). *Results Chem* 7: 101313. https://doi.org/10.1016/j.rechem.2024.101313
35. Hannachi E, Slimani Y, Nawaz M, et al. (2022) Synthesis, characterization, and evaluation of the photocatalytic properties of zinc oxide co-doped with lanthanides elements. *J Phys Chem Solids* 170: 110910. https://doi.org/10.1016/j.jpcs.2022.110910
36. Muthukumaran S, Gopalakrishnan R (2012) Structural, FTIR and photoluminescence studies of Cu doped ZnO nanopowders by co-precipitation method. *Opt Mater* 34: 1946–1953. https://doi.org/10.1016/j.optmat.2012.06.004
37. Arellano-Cortaza M, Ramírez-Morales E, Pal U, et al. (2021) pH dependent morphology and texture evolution of ZnO nanoparticles fabricated by microwave-assisted chemical synthesis and their photocatalytic dye degradation activities. *Ceram Int* 47: 27469–27478. https://doi.org/10.1016/j.ceramint.2021.06.170
38. Tauc J, Menth A (1972) States in the gap. *J Non-Cryst Solids* 8–10: 569–585. https://doi.org/10.1016/0022-3093(72)90194-9
39. Marotti R (2004) Bandgap energy tuning of electrochemically grown ZnO thin films by thickness and electrodeposition potential. *Sol Energy Mater Sol Cells* 82: 85–103. https://doi.org/10.1016/j.solmat.2004.01.008
40. Foo KL, Hashim U, Muhammad K, et al. (2014) Sol–gel synthesized zinc oxide nanorods and their structural and optical investigation for optoelectronic application. *Nanoscale Res Lett* 9: 429. https://doi.org/10.1186/1556-276x-9-429
41. Wong EM, Searson PC (1999) ZnO quantum particle thin films fabricated by electrophoretic deposition. *Appl Phys Lett* 74: 2939–2941. https://doi.org/10.1063/1.123972
42. Urbach F (1953) The long-wavelength edge of photographic sensitivity and of the electronic absorption of solids. *Phys Rev* 92: 1324–1324. https://doi.org/10.1103/PhysRev.92.1324
43. Anyaegbunam FNC, Augustine C (2018) A study of optical band gap and associated urbach energy tail of chemically deposited metal oxides binary thin films. *Dig J Nanomater Bios* 13: 847–856.
44. Liyana GR, Sofyan N, Dhaneswara D, et al. (2020) Optoelectronic properties of ZnO nanorods thin films derived from chemical bath deposition with different growth times. *AIP Conf Proc* 2262: 030008. https://doi.org/10.1063/5.0015869